

Incommensurate magnetic structure and magnetism under pressure in Ho_3Co

Srikanta Goswami ^{1,2,*}, M. I. Sousa Henriques ², V. Petříček ², and P. D. Babu ¹

¹*UGC-DAE Consortium for Scientific Research, Mumbai Centre, BARC Campus, Mumbai - 400085, India*

²*FZU - Institute of Physics of the Czech Academy of Sciences, Na Slovance 1999/2, 182 21 Prague 8, Czechia*



(Received 12 January 2024; revised 22 April 2024; accepted 21 May 2024; published 12 June 2024)

The bulk magnetic measurements (dc magnetization, specific heat, ac-susceptibility) on Ho_3Co suggest that its magnetic structure changes continuously below the Néel temperature $T_N = 21$ K until another antiferromagnetic (AFM) transition takes place at $T_t = 9$ K. In the temperature range $3 \text{ K} \leq T < T_N$, the magnetic structure is described by an incommensurate propagation vector $\mathbf{k} = (\alpha, 0, 0)$ with $0.1605 < \alpha < 0.1585$ and a commensurate component $\mathbf{k}_0 = (0, 0, 0)$. For $T_t < T \leq T_N$, the spin arrangement consists of fanlike and cycloidal modulations for the Ho and Co sublattices, respectively. Below T_t , the presence of the $3\mathbf{k}$ and $5\mathbf{k}$ harmonics results in a highly complex anharmonic ground state associated with the squaring up of the modulation. The evolution of the magnetic modulations in Ho_3Co within $3 \text{ K} \leq T < T_N$ is explained by two active irreducible representations under the $Pnm'a(\alpha 00)000$ magnetic superspace group, which allows the change of the structure without further symmetry breaking. A significant moment contribution is detected in Co. Experiments reveal the coexistence of glassy states, probably related to the complex noncollinear AFM structure at low temperature. In addition, externally applied pressure shifts both transitions at T_N and T_t to higher temperatures. Eventually, high pressure strengthens the AFM interactions at low temperature while the weak glassy states persist up to 1.1 GPa.

DOI: [10.1103/PhysRevB.109.214417](https://doi.org/10.1103/PhysRevB.109.214417)

I. INTRODUCTION

Rare-earth (R) intermetallics, typically forming the archetype of strongly correlated electron systems, exhibit various quantum phenomena originated from complex magnetic interactions and the competition therein. The $4f$ electronic localization crucially emphasizes the low-temperature magnetic states of such systems [1,2]. The binary intermetallics formed with transition metal T (Co, Ni, Rh, Pd) and rich in R , like R_3T or R_5T_2 , exhibit diverse physical properties [3–7]. Field-induced multiple phase transitions and several magnetic transitions with temperature are some of the signature characteristics of these compounds [2,8]. R_3T systems crystallize in orthorhombic $Pnma$ space group, forming a Fe_3C -type structure with two nonequivalent crystallographic sites ($4c$ and $8d$) occupied by the R atoms while the transition metal is at the $4c$ site within the trigonal prisms formed by the rare-earth atoms [5,9,10]. Within this family, Ho_3Co is an interesting case, as it exhibits two different antiferromagnetic (AFM) transitions—one below T_N (~ 21 – 22 K) and the other below T_t (~ 8 – 9 K) [5,11,12]. The transition at T_t was indicated to be of first order due to the formation of an antiferromagnetic nucleus and its growth in the ferromagnetic matrix along the c axis [5]. In another work, Podlesnyak *et al.* reported that the magnetic ordering of Ho_3Co between T_N and T_t has two propagation vectors, $\mathbf{k}_0 = (0, 0, 0)$ and $\mathbf{k}_1 = (0.15, 0, 0)$, and below T_t higher harmonics of \mathbf{k}_1 emerge [11]. Although it can be inferred from the literature [11] that these wave vectors along with the higher harmonics of \mathbf{k}_1 might describe the low-temperature magnetic structure of this compound, an

appropriate solution of the structure does not exist. Thus, despite various studies, this compound still attracts considerable attention for its complex magnetic structures at different temperatures.

Previously it was reported that in the isostructural compound Tb_3Co , a spin-glass-like state coexisted with long-range noncollinear AFM order [7]. The glasslike behavior in that compound was mentioned to originate from the competition between the crystal electric fields (CEFs) and long-range magnetic interactions [7]. To determine whether this spin-glass-like state seen in Tb_3Co is element-independent or is rather a characteristic feature of the R_3T systems, Ho_3Co can possibly be considered for a comparative analysis.

The lattice parameters of Ho_3Co are $a = 6.9516(5)$ Å, $b = 9.2742(8)$ Å, and $c = 6.2138(6)$ Å [13], so that the distance between Co atoms is as large as ~ 4 Å [5,14]. Hence, Ho_3Co might exhibit modulated magnetic properties, due to changes in hybridization between the d and f electronic states, under externally applied hydrostatic pressure (P). Even though the consequence of high pressure on the magnetocaloric effect (MCE) of Ho_3Co is already reported, a detailed discussion on the magnetic behavior under pressure is still lacking [13].

In the present work, the magnetic behavior of Ho_3Co is studied in detail at ambient conditions and under pressure with the aim of a better understanding of the magnetic structure. The spin structure of Ho_3Co and its evolution in the temperature range $3 \text{ K} \leq T < T_N$ are described here. The structure model consists of complex modulations for the Ho and Co magnetic sublattices expressed by two active irreducible representations (*irreps*) allowing extra degrees of freedom under the orthorhombic magnetic superspace group (MSSG). This feature is the key to understanding the substantial changes of the magnetic structure and properties of Ho_3Co . Further,

*goswami@fzu.cz

it is shown that pressure drastically affects the magnetism in this system, and the AFM interactions are strengthened with increasing pressure. Additionally, spin-glass-like states are also shown to coexist in Ho_3Co with an underlying long-range AFM order, even at the highest achieved pressure of 1.10 GPa.

II. EXPERIMENTAL DETAILS

Polycrystalline Ho_3Co was synthesized by arc melting of high-purity Ho and Co (Ho $\sim 99.9\%$ and Co $\sim 99.999\%$) in an argon atmosphere. To achieve better homogenization, the ingot was remelted several times by turning it upside down. Crystalline phase purity was confirmed by x-ray diffraction and neutron powder diffraction (NPD) at room temperature. The NPD pattern was collected in air for a wavelength of $\lambda = 1.48 \text{ \AA}$ and was Rietveld-refined, as shown in the supplemental material (SM) [15] (see also Refs. [16–25] therein). The NPD experiments were performed on the diffractometer FCD-PD-III, which is equipped with position-sensitive detectors, at the Dhruva reactor, BARC, India [26]. The temperature-dependent NPD patterns were collected at $\lambda = 2.315 \text{ \AA}$ at 3, 7, 13, 18, 49, and 102 K by using a closed-cycle refrigerator setup, and the data were analyzed with the help of the program JANA2020 [27,28]. The nuclear contribution coming from the data measured at a paramagnetic temperature (102 K) was subtracted from each diffraction pattern at $T < T_N$. Thus, only the magnetic intensities were used during the refinements. The dc magnetization was measured using a Quantum Design (QD) 9-T physical property measurement system (PPMS) with a vibrating sample magnetometer (VSM), and the pressure-dependent studies were performed in a QD HMD high-pressure cell [29] compatible with VSM. Hydrostatic pressure was transmitted to the sample by Daphne 7373 oil. The applied pressure was monitored via the superconducting transition temperature of a standard Sn manometer. Real and imaginary parts of ac-susceptibility at different frequencies were measured using the ACMS option compatible with the 9 T PPMS. Specific heat was measured on a 14 T Dynacool PPMS that employs relaxation calorimetry with a 2τ approach. Field-dependent specific heat and zero-field data were collected by using a vertical puck made by QD (PPMS application note 1085-156) to incorporate such measurements under high magnetic field for samples with large magnetic moments, like the present one. The specific-heat data were used in our earlier work to calculate the magnetocaloric effect of Ho_3Co [13]. For the magnetic relaxation measurements, the compound was first cooled in the absence of any magnetic field from its paramagnetic state ($\sim 150 \text{ K}$) to the desired temperature, and a magnetic field of 5 T was applied. The field was allowed to stabilize for 1 h before being finally switched off. Subsequently, time-dependent relaxation of magnetization data were collected for 8 h, and the same protocol was used for measurements under different pressure conditions (0.46 and 1.10 GPa).

III. RESULTS

A. dc magnetization

To macroscopically map the magnetic state of Ho_3Co , dc-magnetization (M) was measured in the presence of an applied

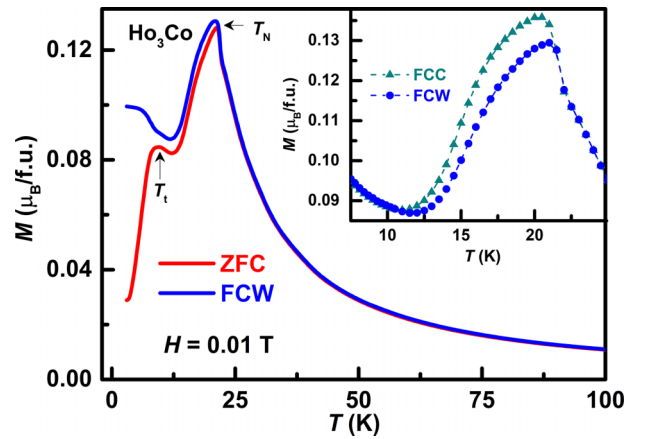


FIG. 1. Temperature-dependent magnetization of Ho_3Co measured in ZFC and FCW under a field of 0.01 T. The arrows indicate the transition temperatures T_N and T_i . The inset shows the thermal hysteresis between the FCC and FCW curves for $T < T_N$.

dc field (H) of 10 mT by following “zero-field-cooled” (ZFC) and “field-cooled-warming” (FCW) paths. The ZFC-FCW results are displayed in Fig. 1 and are in accordance with our earlier work [13]. It is observed that Ho_3Co orders antiferromagnetically below $T_N \sim 21 \text{ K}$ and undergoes another AFM transition at $T_i \sim 9 \text{ K}$, consistent with previous reports [5,11,12]. Upon further cooling, the ZFC curve is found to fall off quickly as temperature tends to 3 K. On the other hand, the FCW curve is seen to deviate from the ZFC curve below T_N , although it follows the ZFC data closely down to 12 K. At this temperature, the FCW curve rises sharply to finally level off as temperature approaches 3 K. Further, when the data were recorded in a cooling (FCC) and a warming cycle under “field-cooled” measurement, a clear thermal hysteresis, indicating the first-order nature of the magnetic transition at T_i , was observed as displayed in the inset of Fig. 1 [5,30,31]. A higher value of effective paramagnetic moment ($\mu_{\text{eff}} = 10.9 \mu_B/\text{Ho}$) than the free ion moment of Ho^{3+} ($10.61 \mu_B$) [1] is obtained upon performing a conventional Curie-Weiss analysis on the high-temperature ZFC curve. Similar higher values of μ_{eff} were already reported and attributed to spin fluctuations originated by $f-d$ exchange in the Co 3d electrons [5].

For further investigation, M versus H virgin isotherms were measured up to $H_{\text{max}} (=9 \text{ T})$ at several temperatures after ZFC from the paramagnetic region (150 K). The data at some selected temperatures are displayed in Fig. S1 in the SM [15]. In the low-field region, weak but clear metamagnetic transitions originating from the AFM interactions can be seen. The full $M-H$ loops are displayed in Fig. 2. Magnetic hysteresis is quite small, and the value of coercivity (H_C) at 3 K is $\sim 0.12 \text{ T}$, which falls off rapidly with increasing temperature. The variation of H_C can be described by the expression $H_C = H_C^0 \exp(-k_B T/\alpha)$ [32], where H_C^0 is the value of H_C at $T = 0$, k_B is Boltzmann’s constant, and α is the parameter measuring the energy barrier needed for the displacement of domain walls. The fitting of $\ln(H_C)$ with temperature is shown in inset (a) of Fig. 2. The slope of the linear fit provides the value of $\alpha = 231.4 \mu\text{eV/K}$. From this parameter, it can be inferred that slight perturbations

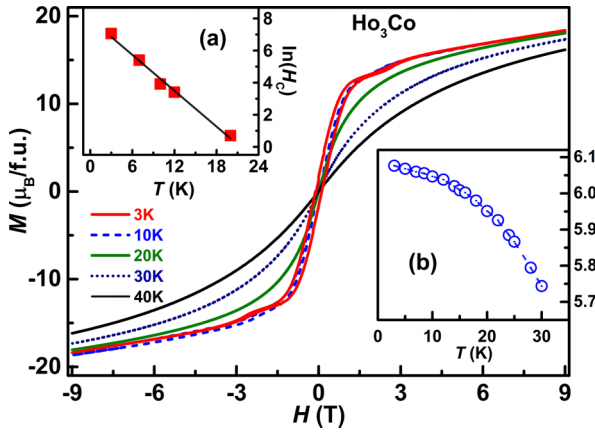


FIG. 2. Isothermal magnetization of Ho_3Co recorded in ZFC mode within ± 9 T at selected temperatures. Variation of coercivity (H_c) with temperature is shown in inset (a). The data were fitted to quantify the stability of domain walls (fitting expression is given in the text). The decreasing nature of the saturation magnetization at 9 T with temperature is shown in inset (b).

might modulate the magnetic domains in this compound. The estimation of the saturation moment per Ho atom at H_{\max} ($\mu_{9\text{T}}/\text{Ho}$) is delineated in the inset (b) of Fig. 2. These values are in good agreement with the saturation moments reported along different crystallographic axes in Ref. [5]. The maximum value of $\mu_{9\text{T}}/\text{Ho}$ ($\sim 6.1 \mu_B/\text{Ho}$) at 3 K gradually decays with increasing temperature. This value corresponds roughly to 57% of the total moment tabulated for the Ho^{3+} free ion [1]. This again signifies that the magnetic moments are not fully aligned in the field direction even in the presence of H_{\max} . Such deviations from the free ion moment values can be caused by strong CEF [33] and by a noncollinear magnetic structure [11]. In fact, our results presented in Sec. III D also show a complex modulation for the spins, which possibly prevents their full alignment.

B. Specific heat

The specific heat (C_p) was measured as a function of temperature for Ho_3Co and the results are presented in Fig. 3. A peak can be seen at T_N , whereas broad humps are observed around T_i (~ 9 K) and at 13.5 K. The peaks in the first derivative of C_p as a function of temperature at zero-field clearly confirm these features for Ho_3Co (see Fig. S2 in the SM [15]). These observations were already reported, but no discussion can be found regarding the hump around 13.5 K [5,17]. However, the magnetic part of specific heat (C_m) was deduced by subtracting the nonmagnetic contributions, i.e., electronic and lattice (phonon) parts from C_p . The nonmagnetic contribution to C_p data, as shown in Fig. 3(a) by a black continuous curve, was obtained by using the full Debye expression [34] along with the electronic contribution given by $C_{\text{el}} = \gamma T$, where γ is the Sommerfeld coefficient. The phonon contribution (C_{ph}) was calculated by using Eq. (1) [34],

$$C_{\text{ph}} \equiv C_{\text{Debye}} = 9nR \left(\frac{1}{\Theta_D} \right)^3 \int_0^{\Theta_D/T} \frac{x^4 e^x}{(e^x - 1)^2} dx, \quad (1)$$

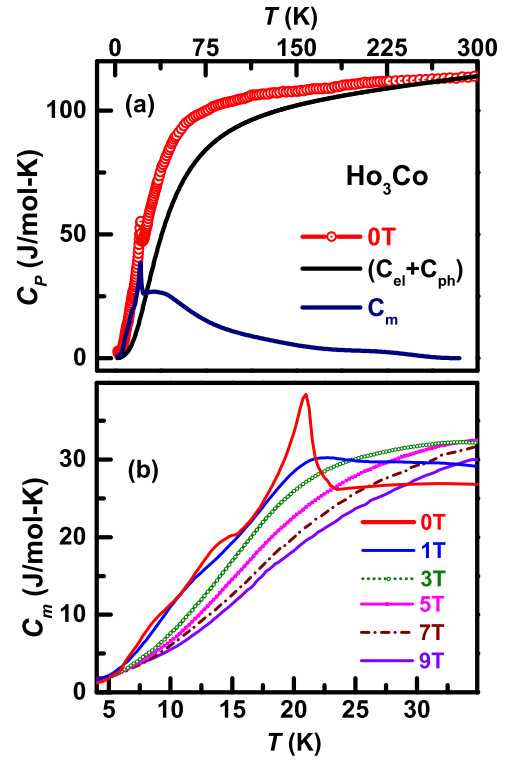


FIG. 3. Calculation of magnetic contribution to the total specific heat of Ho_3Co . The black curve in (a) is the theoretically generated nonmagnetic part of C_p data, whereas the dark blue curve is the estimated magnetic contribution (C_m) in zero-field specific heat. Part (b) displays the low-temperature variation of C_m in the presence of different magnetic fields.

where n is the number of atoms in the formula unit ($n = 4$ for the present case), R is the universal molar gas constant, and Θ_D is the Debye temperature. The estimated magnetic contribution, C_m , is shown in Fig. 3(a) (dark blue curve). Details about the fitting parameters can be found in the SM [15].

Upon application of magnetic field, the peak around T_N is found to be significantly suppressed, as can be seen from Fig. 3(b). In fact, a 1 T field is strong enough to broaden the intense peak. A field increase results in further broadening. The low-temperature humps present in zero-field data vanish in the presence of $H = 3$ T [Fig. 3(b)]. The hump at 13.5 K is not discernible even in the presence of $H = 1$ T, whereas the hump around 9 K is still present at the same field. Though the origin of the hump at 13.5 K is not clear at this point, a careful inspection of the ZFC magnetization and ac-susceptibility data in the following section (see Sec. III C for further details) reveals anomalies at ~ 12.3 K and at ~ 13.5 K, respectively. However, a bulge centered around 17 K can further be seen in the ZFC magnetization curve (Fig. 1), corresponding to a clear hump in the ac-susceptibility data. All these anomalies seem to suggest that either the magnetic structure of this compound is going through a few steps as temperature is lowered from T_N to T_i , or the structure is changing continuously until reaching the state at $T < T_i$. In addition to the above discussion, the neutron diffraction data (see Sec. III D) collected for Ho_3Co suggest that the modulation of the magnetic structure changes,

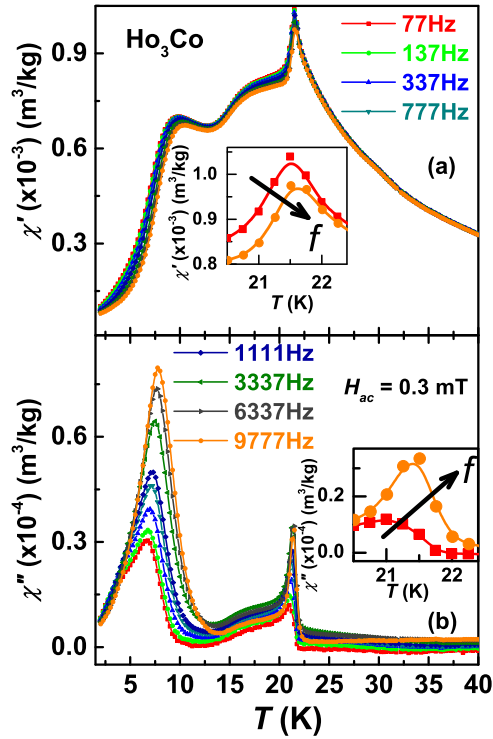


FIG. 4. Temperature dependence of ac-susceptibility data of Ho_3Co : (a) real part χ' , (b) imaginary part χ'' . Data around T_N showing a slight frequency dispersion in ac susceptibility are plotted in the insets.

and the observations in the present work seem to indicate that spins are reorienting further as temperature decreases.

The magnetic contribution in zero-field shows a broad hump persisting beyond T_N and culminating around 35 K. This feature has been attributed to the Schottky-like anomaly and short-range spin correlations [5,17]. At this point, one could investigate the nature of the short-range spin correlations manifested in Ho_3Co . The low value of α from the coercivity analysis of the magnetization data also suggests vulnerable magnetic domains. A general question is whether these short-range spin correlations perturb the long-range magnetic interactions at low temperature in Ho_3Co . To answer this question, studies of ac susceptibility at a low magnetic field were carried out in this compound.

C. ac susceptibility

The real (χ') and imaginary (χ'') parts of the ac susceptibility measured at various frequencies in an ac field (H_{ac}) of 0.3 mT for Ho_3Co are shown in Figs. 4(a) and 4(b). Apart from the peaks around T_N and T_f , a clear dip at 13.5 K and a hump at 17 K are also observed in the χ' data. These additional features have already been discussed in the previous subsection (III B). However, the ac-susceptibility data exhibit clear frequency dispersion around T_N and T_f . The dispersion around T_N was found to be small (~ 0.1 K) compared to the dispersion around T_f (~ 0.7 K). These frequency dispersions seen in the χ' data were further analyzed in a quantitative manner by the following relation: $\phi = \Delta T_f / (T_f \Delta \log f)$ [35,36]. The parameter ϕ , also known as the Mydosh

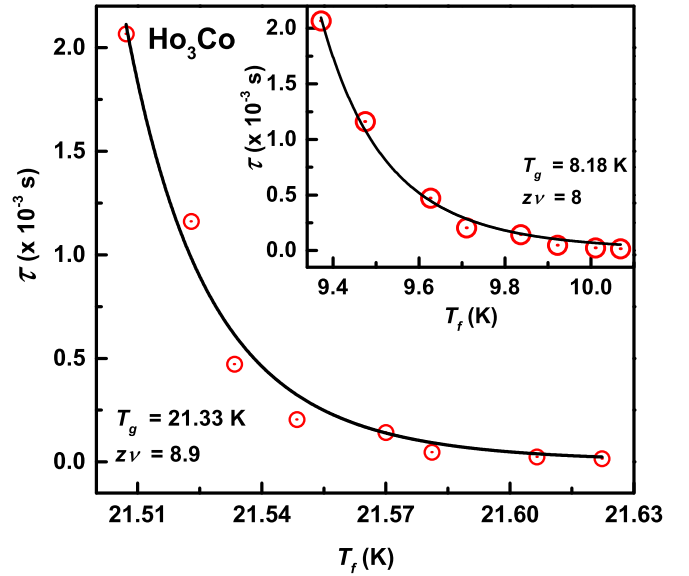


FIG. 5. CSD analyses for two different glassy regions. The fitting protocol is described in the text. The main figure displays the fitting of the data corresponding to the peak around T_N , whereas the inset shows the same for the peak around T_f .

parameter, yields a value of 0.003 for the peak around T_N and 0.035 for the peak around T_f , and it is found to agree well with the values reported for different spin-glass systems [36–38]. In the above expression, T_f is the peak temperature at various frequencies. Here the susceptibility data are analyzed in terms of the “critical slowing down model” (CSD) to check for a possible glasslike behavior [39]. According to this model, the divergence of the relaxation time (τ) as temperature approaches the transition temperature (T_g) is measured and analyzed. T_g is the dc value of $T_f(f)$, i.e., $T_f(f \rightarrow 0)$. Now, the correlation length between the spins (ξ) diverges as $\xi \sim \epsilon^{-\nu}$, where $\epsilon = (T - T_g)/T_g$ is the reduced temperature and ν is the static critical exponent. Further, the relaxation time ($\tau = 2\pi/f$) is related to ξ as $\tau \propto \xi^z$ due to the correlated dynamics, where z is the dynamic critical exponent. Assuming conventional CSD, the relaxation time (τ) can be expressed as Eq. (2) [37,39,40],

$$\tau = \tau_0 \left[\frac{T_f - T_g}{T_g} \right]^{-z\nu}, \quad (2)$$

where T_f is the freezing temperature measured at the peak of χ' , and τ can also be considered as the dynamical fluctuation time, which is comparable to the perception time $t_{\text{obs}} = 1/2\pi f$. Further, τ_0 is the spin flipping time, which is of the order of $\sim 10^{-13}$ s for single spin flip and ranges from $\sim 10^{-12}$ to $\sim 10^{-14}$ s for metallic spin glasses [22,41,42]. The fitting of the data in terms of the above model for the peaks around T_N and T_f is presented in Fig. 5 and its inset, respectively. The parameters estimated from the fitting are tabulated in Table I. The values of $z\nu$, a measure of glassiness, are lying well within the familiar range of 5–10, whereas the value of τ_0 is smaller for the peak at T_N and larger for that at T_f than the expected values for canonical spin-glass materials [20,22,41,42]. The analysis of the χ' data according

TABLE I. Fitting parameters from CSD analysis of χ' data.

T (K)	τ_0 (s)	T_g (K)	$z\nu$
T_N	5.02×10^{-22}	21.33	8.9
T_i	4.40×10^{-10}	8.18	8.0

to the Vogel-Fulcher (VF) law, accurately followed by the interacting spin systems, was also performed and discussed in the SM [15,20]. In addition, the data were checked with the Tholence criteria valid for various spin-glass-like systems, and the results were added to the SM [15,21,23]. All these observations seem to point to the coexistence of glassy states, not exactly canonical spin-glass-like, with antiferromagnetic order driven by Ruderman-Kittel-Kasuya-Yosida (RKKY) interaction at low temperature in this compound. Furthermore, the long-range AFM interactions are always dominating in nature over the interactions forming these glassy states.

D. Neutron powder diffraction

Hereafter, to delve into the microscopic magnetic structure of Ho_3Co , NPD patterns were collected as a function of temperature. The portion of the data below 70° is shown in Fig. 6(a) to emphasize the magnetic contribution to the diffraction patterns. However, the Rietveld refined data up to a higher angle at a paramagnetic temperature (102 K) are shown in Fig. 6(b) [43–45]. Upon cooling the compound from the paramagnetic state [Fig. 6(a)], many additional peaks were found to develop at $T < T_N$ (~ 21 K). It is further noticed that the patterns at $T < T_i$ (~ 9 K) are clearly different from the ones within $T_i < T < T_N$. This points to different magnetic structures in these two regions.

Further, a comparison of the diffraction patterns at 18 and 13 K supports the speculation drawn from other bulk measurements (specific heat, dc-magnetization, and ac-susceptibility) that the magnetic structure is changing within the range $T_i < T \leq T_N$. The most prominent changes in the diffraction patterns collected at these temperatures are shown on the same scale in the inset to Fig. 6(a). Many peaks that were either small or shoulders of other peaks at 18 K are found to develop and be more pronounced at 13 K, such as the ones indicated by * in the inset of Fig. 6(a). This result backs up a somewhat different magnetic structure at 13 K and provides additional support to the findings made from the bulk measurements in earlier sections.

A first attempt to refine the neutron data at 18 K was made by using the wave vectors reported in the literature [11], i.e., $\mathbf{k}_0 = (0, 0, 0)$ and $\mathbf{k}_1 = (0.15, 0, 0)$. The resulting Rietveld fitting of the data was not satisfactory. Thus, a random search for a suitable incommensurate modulation vector was performed in JANA2020 [27,28]. Indeed, new vectors $\mathbf{k}_{18} = (0.1585(19), 0, 0)$ and $\mathbf{k}_{13} = (0.1596(8), 0, 0)$ were obtained for the data at 18 and 13 K, respectively. At this point, the Rietveld refinement showed satisfactory agreement between the experimental data and the calculated pattern at both temperatures, as can be seen in Figs. 7(a) and 7(b) [43–45]. Refinements of the full patterns at these temperatures are

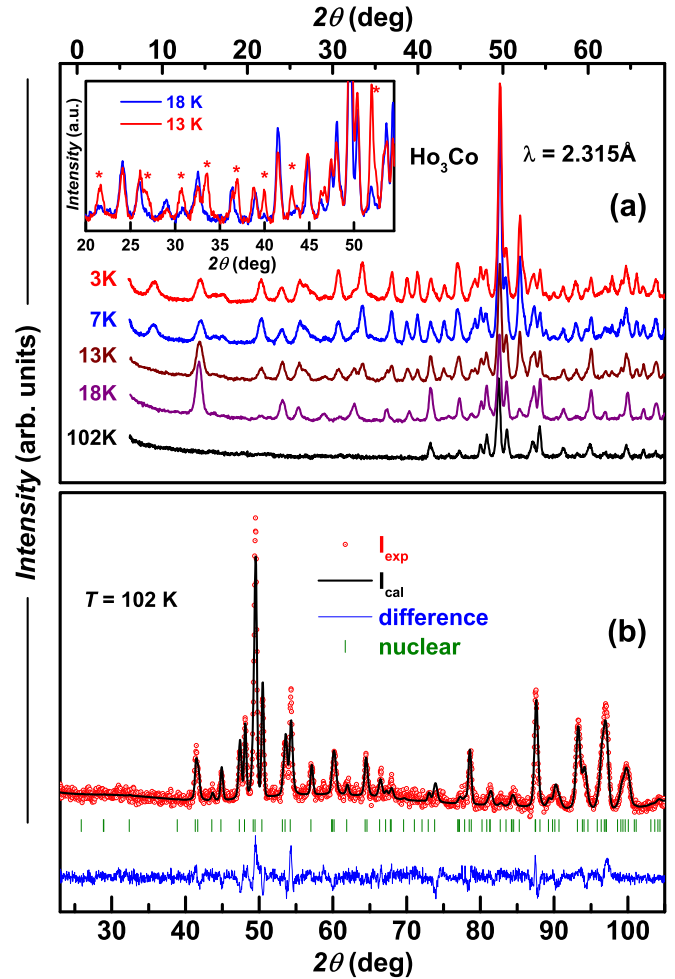


FIG. 6. (a) NPD patterns of Ho_3Co as a function of temperature. The appearance of new peaks at low temperatures is suggestive of the presence of AFM ordering in the system. The changes in magnetic structure within $T_i < T < T_N$ can be seen in the patterns, at 13 and 18 K, with new peaks indicated by *, as shown in the inset. (b) Rietveld refined NPD data at 102 K. The array of vertical lines are the Bragg positions for nuclear reflections.

shown in Fig. S6 in the SM [15]. The fitting factors and the refined parameters are listed in Tables S7– S8 [15].

Representation analysis was performed within the magnetic option of JANA2020. The program calculates the MSSG consistent with the possible active *irreps* for the parent structure and the respective propagation vector(s). Below T_N , the magnetic structure of Ho_3Co has propagation vector $\mathbf{k} = (\alpha, 0, 0)$ with $\alpha \sim 0.16$ (Σ -line of the Brillouin zone) in the parent space group $Pnma$, with Co and Ho1 at $4c$ ($x, 1/4, z$), and Ho2 at $8d$ (x, y, z) (see Table S4 in the SM [15]). The symmetry analysis returned four possible orthorhombic MSSG: $Pnma.1'(\alpha 00)000s$, $Pnma.1'(\alpha 00)0s$, $Pnma.1'(\alpha 00)00ss$, and $Pnma.1'(\alpha 00)0s0s$ for the correspondent *irreps* mSM1, mSM2, mSM3, and mSM4, respectively. The best fit of the experimental data is given by the MSSG $Pnma.1'(\alpha 00)0s0s$ (mSM4), as can be seen in Table S5 in the SM [15]. This model corresponds to cycloidal modulations for the spins of all atoms. However, it was noticed that the experimental intensities of the main reflections were

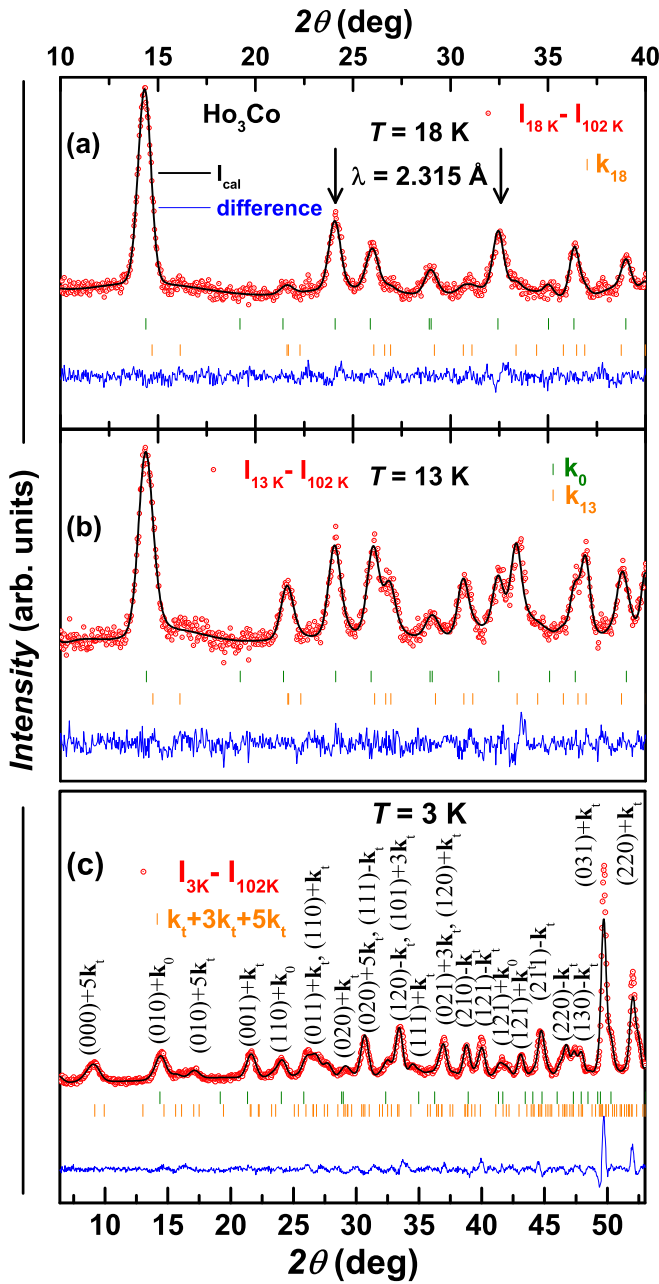


FIG. 7. Rietveld refined NPD data at 18 K (a), 13 K (b), and 3 K (c). The nuclear contribution at 102 K has been subtracted from the experimental data at each temperature. The Bragg positions corresponding to magnetic contribution coming from \mathbf{k}_0 are indicated by the first array of vertical lines (from top), whereas the second set describes the contribution of \mathbf{k}_{18} , \mathbf{k}_{13} (for the data at 18 and 13 K) and \mathbf{k}_1 , $3\mathbf{k}_1$, and $5\mathbf{k}_1$ (for 3 K). The arrows in (a) indicate a significant magnetic contribution from \mathbf{k}_0 . The major contributions to each reflection in (c) are labeled accordingly.

systematically underestimated. That is, a contribution associated with $\mathbf{k}_0 = (0, 0, 0)$ must be considered to improve the fitting of these reflections. This is also in accordance with the previous work [11], where the Γ -point component was used to fit the data. For instance, the calculated structure factor (F^2) for the peaks (1,1,0) and (1,1,1) [indicated by black arrows in Fig. 7(a)] increases from 0 to 20.88 and 11.39, respectively,

by considering the contribution from \mathbf{k}_0 . The refinement factors R_p and R_{obs} for the main reflections at 18 K are 5.3% and 10.2% when not taking into account the \mathbf{k}_0 contribution, whereas with $(\mathbf{k}_{18} + \mathbf{k}_0)$, the same factors are 3.0% and 5.5%, respectively.

The presence of the \mathbf{k}_0 component translates into a decrease in symmetry. The model for the spin configuration realized in Ho_3Co must be a subgroup of the MSSG $Pnma.1'(\alpha 00)0s0s$ that does not contain the symmetry operation $\{1' | 0001/2\}$. The four MSSGs that fulfill this condition are $Pn'm'a(\alpha 00)000$, $Pnm'd'(\alpha 00)000$, $Pn'm'a'(\alpha 00)000$, and $Pnm'a(\alpha 00)000$. Each one of them corresponds, respectively, to a set of two active *irreps* containing the contribution from the Γ -point and the Σ -line modes acting over the spins: $mGM2 + |mSM4$, $mGM3 + |mSM4$, $mGM1 - |mSM4$, and $mGM4 - |mSM4$. The experimental data are best fit by the MSSG $Pnm'a(\alpha 00)000$ (*irreps* $mGM4 - |mSM4$). The agreement factors obtained during the refinements, together with the refined profile parameters and the spin components of the modulation at different temperatures, are listed in Tables S5–S8 in the SM [15].

The magnetic structure of Ho_3Co at 18 K is presented in Fig. 8(i)–8(iv). The point group for the MSSG is $m'mm$ and the magnetic atoms were kept at the same positions compared to the paramagnetic phase. That is, the modulation wave for Ho1 and Co (4c) is forced by symmetry to be in the ac plane. The Ho1 spins are arranged in a fanlike structure [2], with fan spanning of $\sim 100^\circ$ and moment amplitude of $4.1(3)\mu_B$. Any adjacent spin has opposite chirality, as can be seen from Fig. 8(ii). The Ho2 atoms are at their general position, having free spin components in all space directions [Fig. 8(i) and 8(ii)]. In fact, the Ho2 spin modulation is also a fan, but in this case the fan plane is 57° away from the a axis. Any two adjacent Ho2 atoms along the propagation direction are related by an improper twofold rotation, as can be seen from Fig. 8(ii), which shifts the plane and the sense of the spin rotation [Fig. 8(iv)]. The amplitude of the Ho2 spin is $2.72(10)\mu_B$. At the same time, Co spins describe a circular modulation within the ac plane [Fig. 8(iii)], having an amplitude of $1.4(3)\mu_B$. Thus, according to this model the Co atoms do carry a significant moment at 18 K, at variance with previous works on the Ho_3Co structure [5,11,46]. In fact, the refinement factor (R_{obs}) for the satellite reflections improved to 7.42 from 8.10 by allowing a magnetic contribution from the Co atoms. Some reflections for which the calculated magnetic structure factor ($F_c\text{Mag}$) changes the most with the Co magnetic contribution are listed in Table S9.

The other sets of experimental data collected at $T < 18$ K were analyzed similarly to what was described for the set at 18 K. At 13 K, the structure is the same as at 18 K, but with larger magnetic moments [amplitudes of Ho1, Ho2, and Co spins are $6.57(19)\mu_B$, $4.95(15)\mu_B$, and $2.1(2)\mu_B$]. This is in line with the drastic changes in the macroscopic magnetic quantities within $T_i < T \leq T_N$, as discussed in the earlier sections.

For $T < T_i$, the diffraction patterns show some different intensities when compared to the patterns for $T > T_i$ (13 and 18 K data). It can be speculated that the ground-state magnetic structure might be more complex than that between T_N and T_i . Indeed, the appearance of higher harmonics of \mathbf{k}_1 in the

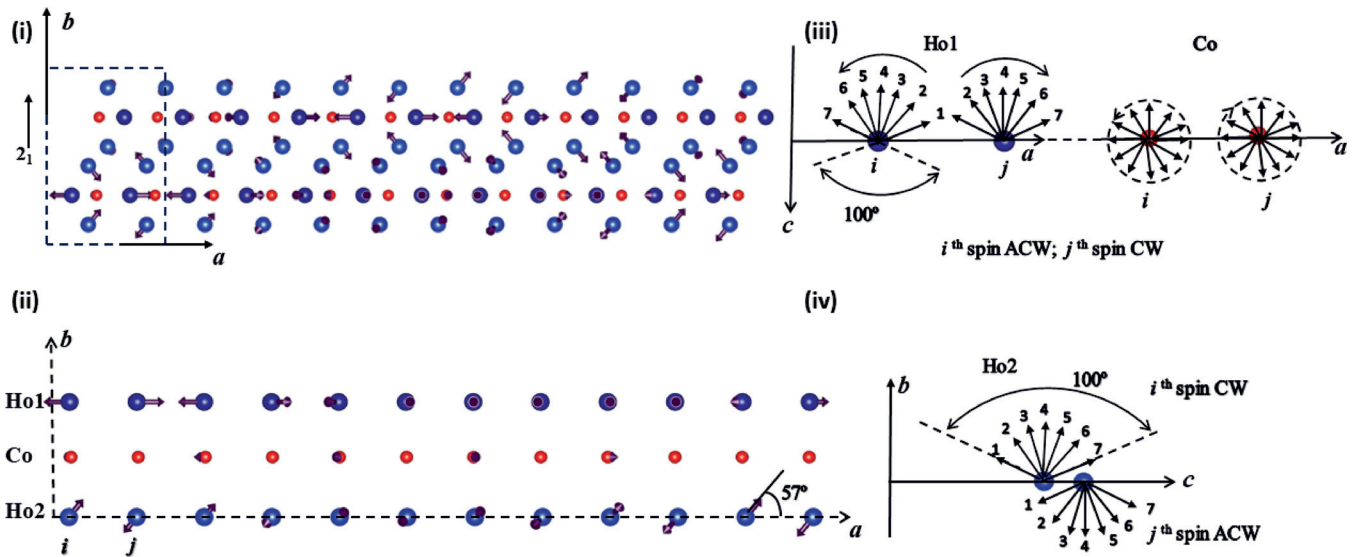


FIG. 8. Magnetic structure of Ho_3Co at 18 K. (i) The spin modulation for Ho1 (dark blue), Ho2 (blue), and Co (red) represented in a $6 \times 1 \times 1$ supercell of the parent orthorhombic unit cell (black arrows with dotted lines); (ii) shows the orientation of the moments for the three sublattices. Ho1 and Co spins are restricted to the ac plane, whereas Ho2 spins are in a plane 57° away from the a axis. Part (iii) shows the fanlike structure for Ho1, where the i th spin moves anticlockwise (ACW) and the j th spin clockwise (CW). Co spins describe a cycloid. Part (iv) displays the fanlike structure for Ho2 spins in which the i th (j th) spin rotates CW (ACW).

temperature range below T_i was reported in the literature [11]. Initially, an attempt was made to solve the structure at 3 K by following the same procedure that was adopted to solve the structures for $T > T_i$. A propagation vector $\mathbf{k}_r = (0.1605(3), 0, 0)$, very close to \mathbf{k}_{13} , was obtained from the random search procedure, but this was not enough to index all the peaks in the pattern. Thus, higher harmonics, i.e., $3\mathbf{k}_r$ and $5\mathbf{k}_r$, were allowed throughout the fitting and refinement of this magnetic structure under the MSSG $Pnm'a(\alpha 00)000$ [25]. The best fit for the subtracted data at 3 K is presented in Fig. 7(c), and a full pattern refinement is also shown in Fig. S7 in the SM [15]. A reasonably good match between the experimental and calculated patterns is seen. The refined parameters and the refinement factors can be found in Tables S7–S8 in the SM [15]. At 3 K the moment modulation in Ho_3Co is no longer sinusoidal but is rather described by a square wave associated with the propagation vector \mathbf{k}_r and its third and fifth harmonics. This is confirmed by plots of the moment amplitude variation across one period of the modulation presented in the SM (Fig. S9) [15]. The contribution of these two harmonics $3\mathbf{k}_r$ and $5\mathbf{k}_r$ to the moment modulation is estimated to be about 13% and 41% of the first harmonic in average amplitude, respectively. The larger contribution from $5\mathbf{k}_r$ can probably be attributed to the clustering of the magnetic moments into certain directions as a consequence of the competition between exchange and anisotropy components of the free energy [47]. A very similar \mathbf{k} vector was obtained by random search for the data at 7 K, thus the same \mathbf{k}_r was used during the refinement.

The analysis done so far provides interesting results. The magnetic state associated with a \mathbf{k} -vector of type $(\alpha, 0, 0)$ with $0.1605 < \alpha < 0.1585$ is always present down to the lowest temperature, and higher-order harmonics combine below T_i to give rise to a complex incommensurate magnetic structure with the squaring up of the modulation. Below T_N ,

the magnetic modulation is continuously strengthened with a decrease of temperature, and finally below T_i it becomes anharmonic and thus minimal changes in the magnetic structure are seen at $T < T_i$. This behavior is quite well explained by the magnetic structure model realized by Ho_3Co under the MSSG $Pnm'a(\alpha 00)000$, which includes two *irrep* modes $m\text{GM}4 - |m\text{SM}4$. The GM-point component associated with $m\text{GM}4 -$ plays a crucial role, as it introduces degrees of freedom to the structure, namely the presence of high-order harmonics. This is rather important as it results in the possibility of continuous change in the magnetic modulation for $T < T_N$ without further need for symmetry breaking down to 3 K. Another outcome is that the moment contribution coming from Co especially for $T \leq 13$ K is quite significant in this compound. At the same time, it can also be remembered that spin fluctuations in $3d$ or $4d$ bands coming from the transition metal through $f-d$ exchange interaction significantly affect the magnetic moments in R_3T compounds [5,48]. An estimate of the effective magnetic moment of Co in terms of such fluctuations was reported by Baranov *et al.*, and it is worth mentioning that the obtained moment values in this section agree well with the magnetization reported for Ho_3Co along different crystallographic axes [5].

E. Magnetization under high pressure

The magnetic nature of Ho_3Co at ambient conditions is explained in detail in the previous sections, and to explore the changes in magnetic behavior of this compound in the presence of high pressure, ZFC magnetization was measured at $H = 0.01$ T in different pressure conditions up to 1.10 GPa, as shown in Fig. 9. It can be noticed from this figure that the behavior of ZFC curves is modulated reasonably upon application of pressure as T_N is found to increase by 9% with $dT_N/dP = 1.40$ K/GPa (inset of Fig. 9). This is quite in

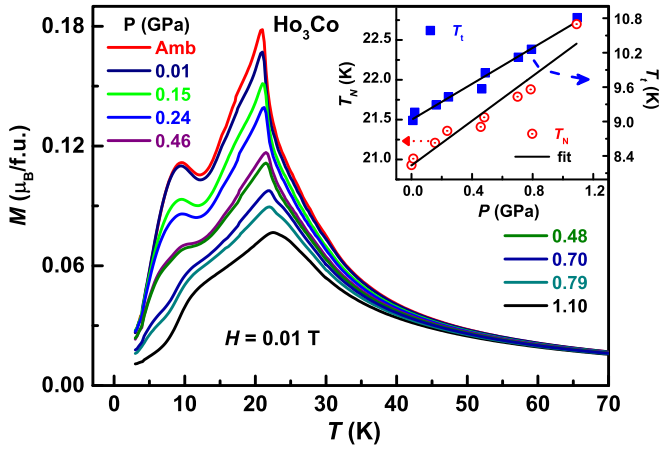


FIG. 9. ZFC magnetization of Ho_3Co recorded at a magnetic field of 0.01 T under applied hydrostatic pressure up to ~ 1 GPa. The inset shows the shift of T_N and T_i with pressure. The black continuous lines correspond to a linear fit to the data.

contrast with that observed in the case of Tb_3Co [49]. However, the reason behind this increase of T_N with pressure may rightly be attributed to the proximity of the spins resulting in an enhancement of ordering temperature with pressure [50]. On the other hand, the AFM transition at T_i is found to be largely modulated by the application of pressure. The intense peak observed at zero pressure is flattened progressively and shifted to higher temperature by 20% as shown in the inset of Fig. 9. The rate of the increase is estimated as $dT_i/dP = 1.55$ K/GPa. Further, the ZFC-FCW data as a function of pressure are displayed in Fig. S11 in the SM [15]. The continuous abolition of the sharp peak at T_i with increasing pressure is again reflected in FCW curves as well.

To delve into more detail, M versus H isotherms were collected as a function of pressure, and the data at selected temperatures are displayed in Fig. S12 in the SM [15]. The significant changes in the shape of the loops from single s-shaped to double s-shaped, especially in the low-field region shown in Fig. S12 [15], indicate conventional collinear AFM-like structure under pressure in this compound. The strengthening of the AFM interactions at low temperature is further supported by the increase of the critical field required for the metamagnetic transition (H_{cr}) with pressure, and the details are furnished in the SM [15].

At this point a small comparison can be made, with an isostructural compound Tb_3Co , for the effect of pressure on the magnetic behavior. It is observed that pressure affects the magnetism in Ho_3Co profoundly at the low-temperature region, whereas in the case of Tb_3Co mostly the higher-temperature region below T_N was affected, and also the magnetic transition temperatures were decreased with increasing pressure [49].

F. Time-dependent magnetization

In the earlier section, it was seen from the ac-susceptibility studies performed that Ho_3Co exhibits glassy states coexisting with long-range AFM order at two different temperatures. This prompted us to perform experiments on magnetic

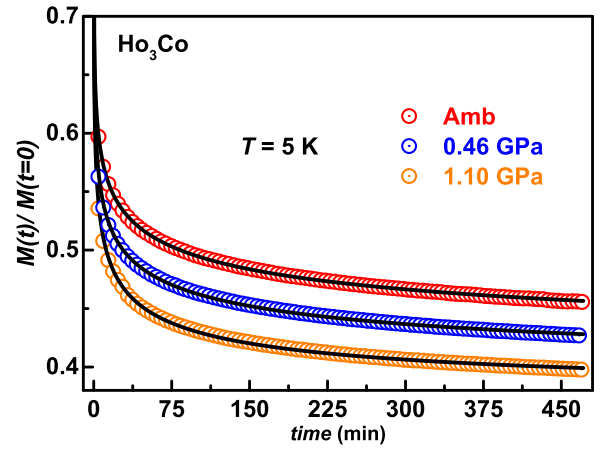


FIG. 10. Relaxation of magnetization for Ho_3Co at different pressures at 5 K. The solid continuous curves represent the fitting of the data to Eq. (3).

relaxation and memory effect under applied pressure to examine the glassiness of this compound. Relaxation of magnetization studies were performed at different temperatures, such as 5 K ($T < T_i$), 16 K ($T < T_N$), and 30 K (paramagnetic region), following ZFC protocol. The measurement convention is already described in the experimental details, and after obtaining the magnetic relaxation, the data $[M(t)]$ were normalized to their value at $t = 0$ (magnetization at $H = 0$), and $M(t)/M(t = 0)$ is finally plotted as a function of time in Fig. 10. The magnetization at 5 K is still relaxing even at the end of 8 h. The relaxation seemed to be faster with increasing pressure as the limiting values of $M(t)/M(t = 0)$ at the end of data collection were found to be 0.46, 0.43, and 0.40 for ambient, 0.46, and 1.10 GPa, respectively. The relaxation at 16 K was much faster and at 30 K it was almost instantaneous, as expected for the data at the paramagnetic region. The data at 5 K were then fitted with the stretched exponential equation, given by Eq. (3):

$$M(t) = M_0 \pm M_g \exp(-t/\tau)^{1-n}, \quad (3)$$

where M_0 describes the intrinsic magnetization, M_g is the glassy component of magnetization, τ is the characteristic relaxation time, and n is the stretching exponent. The \pm sign is indicative of magnetization decay (+) or growth (-). The quantities n and τ both depend on temperature. The value of n varies in $[0, 1]$, where 1 implies no relaxation and 0 indicates relaxation with a single relaxation time. The values of τ and n from the fitting of $M(t)/M(t = 0)$ data to Eq. (3) are tabulated in Table II.

TABLE II. Parameters obtained from the fitting of magnetic relaxation data at 5 K to Eq. (3).

P (GPa)	τ (s)	n
Ambient	78	0.841
0.46	33	0.840
1.10	21	0.817

The value of τ at ambient conditions is only 78 s, although it should be \sim thousands of seconds for a canonical spin-glass system [51]. Thus, the glasslike character in this compound is very weak and far from any canonical spin glass, even compared to the other isostructural compound Tb_3Co [7,49]. If the measurement were taken at 2 K instead of 5 K, then a higher value of τ could have been expected, as 5 K is closer to the glass temperature associated with the transition at T_f . However, the value of n agrees well with the values found for other spin-glass systems [52]. Moreover, the values of τ and n are found to decrease with increasing pressure. This suggests that the weak glassy states found in Ho_3Co at ambient condition are further weakened by external pressure. Additional support for the existence of the glassy states is obtained from the magnetic memory effect experiments [24] at different pressure conditions (see the SM [15]).

IV. DISCUSSION

The results presented here uncover further the complex magnetic order in Ho_3Co . AFM helical structures result from the interplay between competing exchange interactions in the system. Furthermore, in the absence of external magnetic fields, the features of the helix (helices) depend on the magnetocrystalline anisotropy emerging from the structure and symmetry of a particular compound. The long-range RKKY exchange interaction and its competition with the low-symmetry CEF particularly influence the magnetic behavior in this compound [5]. The CEF effect is also reflected in the Schottky-like anomaly in the C_p data. The temperature variation of C_p under applied magnetic fields together with dc and/or ac magnetization suggest a change in the magnetic structure between T_N and T_f . In fact, the description of the incommensurate magnetic modulation of Ho_3Co under the MSSG $Pnm'a(\alpha 00)000$ confirms it. This MSSG corresponding to two active magnetic *irrep* modes intrinsically introduces higher-order harmonic degrees of freedom associated with an important \mathbf{k}_0 contribution, allowing the noticeable changes of the magnetic structure without further symmetry breaking at T_f . Moreover, below T_N this zero-field model reproduces the magnetization curves for Ho_3Co measured along the main crystallographic directions at a 5 mT field in a previous work (Ref. [5], Fig. 1). It is also consistent with the magnetization dynamics involving spin rotation to align with the applied field along the main crystallographic directions [5].

Fanlike structures are commonly found in field-dependent phase diagrams of antiferromagnetic materials for intermediate applied fields which break the zero-field helical structure. The fanlike structure realized by the Ho2 sublattice at 18 K is quite curious, and probably some geometric frustration is also at play here. As shown in Fig. S10 in the SM [15], the Ho2 spins are left to rotate in a plane that is 57° away from Ho1, and very close to the Ho2-Ho1 dihedral bond angles (60°) in the distorted tetrahedral space along the propagation direction. Initially, the sequence of spins is two Ho2 in and two Ho1 out alternating two Ho2 out and two Ho1 in the next distorted tetrahedra along the modulation direction. This sequence seems to be perturbed by the Ho1 rotation in the *ac* plane, which is symmetry-protected, sustaining the modulation as some lattice period is needed for the spins to

reach again a more stable configuration. Another important outcome is that below the second magnetic transition at T_f , the anharmonic nature of modulation manifests itself by the presence of $3\mathbf{k}$ and $5\mathbf{k}$ harmonics. Interestingly, Ho metal also exhibits a distorted helical magnetic structure at low temperature which is governed by 5th and 7th harmonics of the primary modulation [53]. In reference to the squaring-up process, the emergence of the third harmonic is also evident in the case of Ho_7Rh_3 [54]. The squaring up of the modulation wave of a magnetic structure is a mechanism of lowering the energy of the system while keeping an incommensurate modulation. In general, a system at low temperature either undergoes a transition to a stable commensurate magnetic structure or remains in an incommensurate magnetic structure by squaring up of the modulation leading to the emergence of higher-order harmonics [55,56].

The complex noncollinear magnetic structure along with strong magnetic anisotropy [5] probably plays a crucial role behind the formation of spin-glass states at low temperature. Despite the long-ranged periodic order, the single-ion anisotropy could further tilt the spins at the local level such that any of its components can randomly be frozen. This frustration may be attributed to the random freezing of some spin components to finally develop short-range magnetic interactions leading to spin-glass-like states at low temperature in this compound. This is also in line with the existence of some possible geometric frustration. The external pressure, on the other hand, possibly modifies the distance between nearest atoms ($\sim 3.5 \text{ \AA}$), which in turn increases the probability of more interactions, frustrations, and the freezing of components of spins. Nevertheless, no direct evidence is found in terms of diffuse scattering in neutron diffraction [36]. One plausible explanation is that the disorder, responsible for originating the short-range magnetic interactions in a system, should be strong enough to be reflected in NPD. The absence of diffuse scattering in neutron diffraction is also reported for many magnetic compounds with coexisting spin-glass states, such as Tb_2PdSi_3 and Dy_2CuIn_3 [57,58]. However, the observation of memory effects can be held as another piece of confirmative evidence for the spin-glass dynamics irrespective of its origin to enact canonical spin-glasses or if the dynamical nature of spins is originated by intercluster interactions [24,59]. Relaxation of magnetization and memory effects have been observed in canonical spin-glass systems, and according to the droplet model the growth of domains of correlated spins particularly governs this behavior [60,61]. Relative spin orientations in different domains situated at a distance larger than a characteristic length are quite sensitive to small perturbation in temperature, and thus further growth of domains occurs [61].

Contrary to the literature [4–7,62], a significant moment contribution from Co is detected in this work. It is hard to rule out from the present data whether this moment is induced by *f-d* exchange interaction in the *d*-electron subsystem [4–7,48] or by the modulation involved with the noncollinear magnetic structure. The Co atoms and Ho1 atoms being at the same crystallographic position have the same symmetry restrictions derived for the spin directions. This fact has two direct implications: first, the influence of the dynamics of the Ho1 spin modulation and the respective local field over the

Co spin cannot be discarded; second, the contribution from the Co sublattice alone cannot be disentangled from Ho1 by means of powder diffraction techniques. The additional moment calculated for Ho in Ho₃Co [5] and attributed to $f-d$ exchange in the d -electron subsystem in the transition metal [5,48] is *de facto* the contribution from the Co sublattice. The enhancement of the μ_{eff} at several temperatures was estimated by Baranov *et al.* [5] to be around $1 \mu_B/\text{f.u.}$, which is consistent with the values refined for the Co spin in the present work. Information from element-specific experiments, such as x-ray magnetic dichroism or resonant elastic x-ray scattering performed on single crystals, would be invaluable not only to unambiguously comment on the origin of the moment contribution from the Co sublattice, but also to clarify other aspects of the magnetism in Ho₃Co. Magnetic diffuse scattering, the role of high-order harmonics, the angular dependence of the magnetization, and magnetoelastic couplings are aspects to be exploited in order to gain further insight into the nature of the incommensurate magnetic structure of this compound.

V. CONCLUSIONS

A detailed magnetic study on Ho₃Co was carried out based on dc magnetization, specific heat, ac-susceptibility, and neutron powder diffraction. The dc magnetization was also

performed under pressure up to ~ 1 GPa. The macroscopic measurements show a continuous change in the magnetic structure within $T_i < T \leq T_N$. Microscopic analysis of the magnetic structure confirms this speculation. In fact, the active *irreps* mSM4 and mGM4- under the magnetic super-space group $Pnm'a(\alpha 00)000$ allow the presence of higher harmonics (3k and 5k) for the modulation. This is the key to explaining the continuous changes in the magnetic structure and properties of Ho₃Co with decreasing temperature. The magnetic configuration within $T_i < T \leq T_N$ consists of fanlike (Ho) and cycloidal (Co) modulations. The magnetic modulation strengthens as temperature decreases from T_N to T_i , where the higher harmonics emerge. The anharmonic nature of the magnetic modulation is kept down to 3 K, and is described by a square wave. The magnetic contribution coming from the transition metal, Co, is quite significant at low temperatures. Externally applied hydrostatic pressure completely wipes out the transition at T_i . High-pressure further strengthens the AFM interactions, profoundly affecting the magnetism at low temperature. Moreover, noncanonical glassy states, which probably originated from some geometric frustration caused by complex magnetic structure together with single-ion anisotropy, coexist at low temperature in this compound with dominating long-range noncollinear antiferromagnetic order, irrespective of pressure.

-
- [1] J. Jensen and A. R. Mackintosh, *Rare Earth Magnetism: Structures and Excitations* (Clarendon, Oxford, 1991).
- [2] K. H. J. Buschow, Intermetallic compounds of rare-earth and 3d transition metals, *Rep. Prog. Phys.* **40**, 1179 (1977).
- [3] A. F. Gubkin, E. A. Sherstobitova, P. B. Terentyey, A. Hoser, and N. V. Baranov, A cluster-glass magnetic state in R₅Pd₂ (R = Ho, Tb) compounds evidenced by AC-susceptibility and neutron scattering measurements, *J. Phys.: Condens. Matter* **25**, 236003 (2013).
- [4] N. V. Baranov, A. F. Gubkin, A. P. Vokhmyanin, A. N. Pirogov, A. Podlesnyak, L. Keller, N. V. Mushnikov, and M. I. Bartashevich, High-field magnetization and magnetic structure of Tb₃Co, *J. Phys.: Condens. Matter* **19**, 326213 (2007).
- [5] N. V. Baranov, T. Goto, G. Hilscher, P. E. Markin, H. Micher, N. V. Mushnikov, J. G. Park, and A. A. Yermakov, Irreversible field-induced magnetic phase transitions and properties of Ho₃Co, *J. Phys.: Condens. Matter* **17**, 3445 (2005).
- [6] A. F. Gubkin, L. S. Wu, S. E. Nikitin, A. V. Suslov, A. Podlesnyak, O. Prokhenko, K. Prokes, F. Yokaichiya, L. Keller, and N. V. Baranov, Field-induced magnetic phase transitions and metastable states in Tb₃Ni, *Phys. Rev. B* **97**, 134425 (2018).
- [7] S. Goswami, P. D. Babu, and R. Rawat, Magnetic glassy behaviour coupled with long range non-collinear magnetic order in Tb₃Co, *J. Phys.: Condens. Matter* **31**, 445801 (2019).
- [8] D. Gignoux, F. Givord, R. P. de la Bathie, and F. Sayetat, Magnetic properties and spontaneous distortion in TbCo₂, *J. Phys. F* **9**, 763 (1979).
- [9] K. H. J. Buschow and A. S. Van Der Goot, The crystal structure of rare-earth cobalt compounds of the type R₃Co, *J. Less-Common Met.* **18**, 309 (1969).
- [10] O. A. W. Strydom and L. Alberts, The structure of Gd₃Co, *J. Less-Common Met.* **22**, 511 (1970).
- [11] A. Podlesnyak, A. Daoud-Aladine, O. Zaharko, P. Markin, and N. V. Baranov, Magnetic structures and magnetic phase transitions in Ho₃Co, *J. Magn. Magn. Mater.* **272-276**, 565 (2004).
- [12] J. Shen and J. F. Wu, Magnetocaloric effect and magnetic phase transition in Ho₃Co, *J. Appl. Phys.* **109**, 07A931 (2011).
- [13] S. Goswami, P. D. Babu, and R. Rawat, High pressure study of magnetocaloric effect in Ho₃Co and Tb₃Co, *J. Phys.: Condens. Matter* **32**, 365803 (2020).
- [14] E. Talik and M. Neuman, XPS investigations of Y₃Ni and Gd₃Ni single crystals, *Phys. B: Condens. Matter* **193**, 207 (1994).
- [15] See Supplemental Material at <http://link.aps.org/supplemental/10.1103/PhysRevB.109.214417> for additional analysis and crystallographic details on magnetic refinements.
- [16] O. V. Lounasmaa, Specific heat of holmium metal between 0.38 and 4.2° K, *Phys. Rev.* **128**, 1136 (1962).
- [17] T. Palewski, N. V. Tristan, K. Nenkov, K. Skokov, and S. A. Nikitin, Magnetization and specific heat of the Ho₃Co compound, *J. Magn. Magn. Mater.* **258-259**, 561 (2003).
- [18] J. S. Nowak, B. Wiendlocha, K. Holowacz, P. Reczek, M. Podgorski, M. J. Winiarski, and T. Klimczuk, Fermi-liquid behavior of binary intermetallic compounds Y₃M (M = Co, Ni, Rh, Pd, Ir, Pt), *Mater. Res. Express* **4**, 066501 (2017).
- [19] N. V. Tristan, K. Nenkov, K. Skokov, and T. Palewski, Specific heat and magnetic susceptibility of intermetallic compounds R₃Ni, *Phys. B: Condens. Matter* **344**, 462 (2004).
- [20] J. Souletie and J. L. Tholence, Critical slowing down in spin glasses and other glasses: Fulcher versus power law, *Phys. Rev. B* **32**, 516(R) (1985).

- [21] K. Gornicka, K. K. Kolincio, and T. Klimczuk, On the frequency dependence of the transition temperature in spin glasses, *Intermetallics* **100**, 63 (2018).
- [22] R. Laiho, E. Lahderanta, J. Salminen, K. G. Lisunov, and V. S. Zakhvalinskii, Spin dynamics and magnetic phase diagram of $\text{La}_{1-x}\text{Ca}_x\text{MnO}_3$ ($0 < x < 0.15$), *Phys. Rev. B* **63**, 094405 (2001).
- [23] J. L. Tholence, On the frequency dependence of the transition temperature in spin glasses, *Solid State Commun.* **35**, 113 (1980).
- [24] Y. Sun, M. B. Salamon, K. Garnier, and R. S. Averback, Memory effects in an interacting magnetic nanoparticle system, *Phys. Rev. Lett.* **91**, 167206 (2003).
- [25] J. M. Perez-Mato, J. L. Ribeiro, V. Petricek, and M. I. Aroyo, Magnetic superspace groups and symmetry constraints in incommensurate magnetic phases, *J. Phys.: Condens. Matter* **24**, 163201 (2012).
- [26] A. V. Pimpale, B. A. Dasannacharya, V. Siruguri, P. D. Babu, and P. S. Goyal, Neutron powder diffractometer beam line with a toroidally bent asymmetric crystal monochromator: Monte Carlo simulation studies, *Nucl. Instrum. Methods* **481**, 615 (2002).
- [27] V. Petříček, M. Dušek, and L. Palatinus, Crystallographic computing system JANA2006: General features, *Z. Kristallogr.* **229**, 345 (2014).
- [28] V. Petříček, L. Palatinus, J. Plášil, and M. Dušek, JANA2020 - a new version of the crystallographic computing system JANA, *Z. Kristallogr.* **238**, 271 (2023).
- [29] Pressure cell for magnetometry, https://www.qdusa.com/siteDocs/productBrochures/1084-500_PPMS_HPC.pdf.
- [30] J. Iida, Y. Nakagawa, and N. Kimizuka, Field-heating effect-anomalous thermomagnetization curves observed in hexagonal LuFe_2O_4 , *J. Phys. Soc. Jpn.* **55**, 1434 (1986).
- [31] V. Markovich, I. Fita, A. Wisniewski, R. Puzniak, C. Martin, G. Jung, and G. Gorodetsky, Phase transitions and magnetic properties of LuFe_2O_4 under pressure, *Phys. Rev. B* **96**, 054416 (2017).
- [32] A. V. Deryagin, N. V. Baranov, and V. A. Reimer, Magnetic properties and magnetic transitions in rare-earth intermetallic compounds $(\text{Tb}_{1-x}\text{Y}_x)_3\text{Co}$, *Zh. Eksp. Teor. Fiz.* **73**, 1389 (1977) [*Sov. Phys. JETP* **46**, 731 (1977)].
- [33] R. J. Radwański and N. H. Kim-Ngan, The crystal field and exchange interactions in NdNi_5 , UGa_2 and UPd_2Al_3 , *J. Alloys Compd.* **219**, 260 (1995).
- [34] E. S. R. Gopal, *Specific Heat in Low Temperature* (Plenum, New York, 1966).
- [35] S. Sullow, G. J. Nieuwenhuys, A. A. Menovsky, J. A. Mydosh, S. A. M. Mentink, T. E. Mason, and W. J. L. Buyers, Spin glass behavior in URh_2Ge_2 , *Phys. Rev. Lett.* **78**, 354 (1997).
- [36] J. A. Mydosh, *Spin Glasses: An Experimental Introduction* (Taylor and Francis, London, 1993).
- [37] L. Dormann, L. Bessais, and D. Fiorani, A dynamic study of small interacting particles: Superparamagnetic model and spin-glass laws, *J. Phys. C* **21**, 2015 (1988).
- [38] K. Binder and A. P. Young, Spin glasses: Experimental facts, theoretical concepts, and open questions, *Rev. Mod. Phys.* **58**, 801 (1986).
- [39] P. C. Hohenberg and B. I. Halperin, Theory of dynamic critical phenomena, *Rev. Mod. Phys.* **49**, 435 (1977).
- [40] N. Marcano, P. A. Algarabel, L. F. Barquin, J. P. Araujo, A. M. Pereira, J. H. Belo, C. Magen, L. Morellon, and M. R. Ibarra, Cluster-glass dynamics of the Griffiths phase in $\text{Tb}_{5-x}\text{La}_x\text{Si}_2\text{Ge}_2$, *Phys. Rev. B* **99**, 054419 (2019).
- [41] K. Gunnarsson, P. Svedlindh, P. Nordblad, L. Lundgren, H. Aruga, and A. Ito, Dynamics of an Ising spin-glass in the vicinity of the spin-glass temperature, *Phys. Rev. Lett.* **61**, 754 (1988).
- [42] J. Mattsson, T. Jonsson, P. Nordblad, H. A. Katori, and A. Ito, No phase transition in a magnetic field in the Ising spin glass $\text{Fe}_{0.5}\text{Mn}_{0.5}\text{TiO}_3$, *Phys. Rev. Lett.* **74**, 4305 (1995).
- [43] H. M. Rietveld, Line profiles of neutron powder-diffraction peaks for structure refinement, *Acta Cryst.* **22**, 151 (1967).
- [44] H. M. Rietveld, A profile refinement method for nuclear and magnetic structures, *J. Appl. Cryst.* **2**, 65 (1969).
- [45] R. A. Young, *The Rietveld Method* (Oxford University Press, Oxford, 1993).
- [46] D. Gignoux, J. C. Gomez-Sal, and D. Paccard, Magnetic properties of a Tb_3Ni single crystal, *Solid State Commun.* **44**, 695 (1982).
- [47] J. A. Paixão, M. Ramos Silva, S. Aa. Sørensen, B. Lebech, G. H. Lander, P. J. Brown, S. Langridge, E. Talik, and A. P. Gonçalves, Neutron-scattering study of the magnetic structure of DyFe_4Al_8 and HoFe_4Al_8 , *Phys. Rev. B* **61**, 6176 (2000).
- [48] N. V. Baranov, K. Inoue, H. Michor, G. Hilscher, and A. A. Yermakov, Spin fluctuations in Gd_3Rh induced by f-d exchange: The influence on the T -linear specific heat, *J. Phys.: Condens. Matter* **15**, 531 (2003).
- [49] S. Goswami, P. D. Babu, and R. Rawat, High pressure study of magnetic properties of Tb_3Co , *J. Phys.: Condens. Matter* **31**, 505802 (2019).
- [50] C. H. Woodall, G. A. Craig, A. Prescimone, M. Misek, J. Cano, J. Faus, M. R. Probert, S. Parsons, S. Moggach, J. Martínez-Lillo, M. Murrice, K. V. Kamenev, and E. K. Brechin, Pressure induced enhancement of the magnetic ordering temperature in rhenium (IV) monomers, *Nat. Commun.* **7**, 13870 (2016).
- [51] D. X. Li, Y. Shiokawa, Y. Homma, A. Uesawa, A. Donni, T. Suzuki, Y. Haga, E. Yamamoto, T. Honma, and Y. Onuki, Evidence for the formation of the spin-glass state in U_2PdSi_3 , *Phys. Rev. B* **57**, 7434 (1998).
- [52] D. Chu, G. G. Kenning, and R. Orbach, Dynamic measurements in a Heisenberg spin glass: CuMn , *Phys. Rev. Lett.* **72**, 3270 (1994).
- [53] W. C. Koehler, Magnetic properties of rare-earth metals and alloys, *J. Appl. Phys.* **36**, 1078 (1965).
- [54] A. F. Gubkin, A. A. Vaulin, T. Tsutaoka, A. F. Prekul, K. P. Skokov, and N. V. Baranov, Magnetic incommensurability, short-range correlations, and properties of Ho_7Rh_3 , *Phys. Rev. B* **106**, 134419 (2022).
- [55] P. Morin, D. Schmitt, and C. Vettier, Squaring-up of modulated magnetic structures in HoAg and TmAg , *J. Phys.* **46**, 39 (1985).
- [56] J. A. Blanco, B. Fak, E. Ressouche, B. Grenier, M. Rotter, D. Schmitt, J. A. Rodríguez-Velamazán, J. Campo, and P. Lejay, Magnetic field and temperature dependence of the amplitude-modulated magnetic structure of PrNi_2Si_2 determined by single-crystal neutron diffraction, *Phys. Rev. B* **82**, 054414 (2010).
- [57] A. Szytula, M. Hofmann, B. Penc, M. Slaski, S. Majumdar, E. Sampathkumaran, and A. Zygmunt, Magnetic behaviour of

- R_2PdSi_3 compounds with $R = Ce, Nd, Tb-Er$, *J. Magn. Magn. Mater.* **202**, 365 (1999).
- [58] I. Siouris, R. Kremer, and M. Hoelzel, Antiferromagnetic order and spin glass behavior in Dy_2CuIn_3 , *J. Magn. Magn. Mater.* **323**, 2903 (2011).
- [59] F. Rivadulla, M. A. Lopez-Quintela, and J. Rivas, Origin of the glassy magnetic behavior of the phase segregated state of the perovskites, *Phys. Rev. Lett.* **93**, 167206 (2004).
- [60] L. Lundgren, P. Svedlindh, P. Nordblad, and O. Beckman, Dynamics of the relaxation-time spectrum in a CuMn spin-glass, *Phys. Rev. Lett.* **51**, 911 (1983).
- [61] D. De, S. Goswami, and M. Chakraborty, Magnetic memory effect: Unfolding magnetic metastabilities, *J. Magn. Magn. Mater.* **565**, 170175 (2023).
- [62] E. Talik, Magnetic and transport properties of the R_3Ni system ($R = Y, Gd, Tb, Dy, Ho, Er$), *Phys. B: Condens. Matter* **193**, 213 (1994).